Electronic Supplementary Material (ESI) for Journal of Materials Chemistry A

A Thermally and Mechanically Stable Solar Cell Made of a Small-Molecule Donor and Polymer Acceptor

Sora Oh,[a,c]† Sachin Badgujar,[a]† Da Hun Kim,[b,c] Wang-Eun Lee,[c,d] Nasir Khan,[b,c] Muhammad Jahandar,[b,c] Shafket Rasool,[a,c] Chang Eun Song,*[,b,c] Hang Ken Lee,[b] Won Suk Shin,[b,c] Jong-Cheol Lee,[a,c] Sang-Jin Moon,[b,c] and Sang Kyu Lee,*[,a,c]

[a]Advanced Materials Division, Korea Research Institute of Chemical Technology (KRICT), 141 Gajeongro, Yuseong, Daejeon 34114, Republic of Korea. E-mail: skyulee@krict.re.kr
[b]Center of Solar Energy Materials, Korea Research Institute of Chemical Technology (KRICT), 141 Gajeongro, Yuseong, Daejeon 34114, Republic of Korea. E-mail: songce@krict.re.kr
[c]Advanced Materials and Chemical Engineering, University of Science and Technology (UST), 217 Gajeongro, Yuseong, Daejeon 34113, Republic of Korea.
[d]Reliability Assessment Center for Chemical Materials, Korea Research Institute of Chemical Technology (KRICT), 141 Gajeongro, Yuseong, Daejeon 34114, Republic of Korea.

† These authors contributed equally.

Correspondence and requests for materials should be addressed to C.E.S. (email: songce@krict.re.kr) or to S.K.L. (email: skyulee@krict.re.kr).

Experimental Sections

Instruments

UV-vis absorption measurements were recorded using double-beam Shimadzu UV–2550 (wavelength range 300–900 nm). The thickness and roughness of films were examined with an Alpha-Step IQ surface profiler (KLA Tencor). The atomic force microscope (AFM) (Multimode IIIa, Digital Instruments) was operated in tapping mode to acquire images of the surfaces of films. Cross-sectional TEM image of thick devices were acquired by iusing a Helios dual Beam FIB. Conventional transmission electron microscopy (TEM) was performed using a JEOL JEM-2200FS. FE-SEM was performed on Tescan Mira 3 LMU FEG operated at 20 kV. X-ray photoelectron was performed on AXIS Nova (150 W, monochromatic Al-Kα, 40 eV). The *J-V* characteristics of relevant devices were measured by using a computer-controlled Keithley 236 source measure unit.

Materials

All chemicals and solvents were purchased from Aldrich and were used without further purification. The materials BDT2TR was synthesized by this literature[1], $PC_{71}BM$ and PNDI-2T were purchased from EM-Index and one-materials, respectively.

Fabrication of the Organic solar cells (OSCs)

In this study, the devices were fabricated with the structure ITO/PEDOT:PSS/ BDT2TR small molecule donor:$PC_{71}BM$ or PNDI-2T acceptor/Ca/Al. The procedure for cleaning the ITO surface included sonication and rinsing in deionized water, methanol, and acetone. The PEDOT:PSS (~35nm) film as a hole transport layer was spin-coated onto each ITO anode from a solution purchased from H. C. Starck (AI 4083). For deposition of the active layer, blend solutions of BDT2TR:$PC_{71}BM$, BDT2TR:PNDI-2T (1.0:1.0 w/w, 15 mg, filtered by 0.45μm) dissolved in chloroform (1 mL) were spin-cast (at 2000 r.p.m.) on top of the PEDOT:PSS layer.

The optimized thickness of active layer was ~ 100nm. From thicker to thinner films were produced by varying the solution concentration and spin rate from total 1.2 to 3.0 wt% and from 600 to 4000 r.p.m. After the deposition of photo-active layers all substrates were dried on hot plate for 10min at 100 ^{o}C. Calcium and aluminum contacts were formed by vacuum deposition at pressures below 3 x 10^{-6} Torr, providing an effective active area of 0.09 cm^2. Solar cell efficiencies were characterized under simulated 100 mW/cm^2 AM 1.5G irradiation from a Xe arc lamp with an AM 1.5 global filter. Simulator irradiance was characterized using a calibrated spectrometer, and the illumination intensity was set using an NREL-certified silicon diode with an integrated KG1 optical filter. The EQE was measured by underfilling the device area using a reflective microscope objective to focus the light output from a Xenon lamp outfitted with a monochromator and optical chopper; the photocurrent was measured using a lock-in amplifier, and the absolute photon flux was determined using a calibrated silicon photodiode. All device fabrication procedures and measurements were carried out in air at room temperature.

Solar cell stability

Thermal stability test: all devices fabricated as follow organic solar cell fabrication process. But before deposition of top electrode (Ca/Al), the films were placed on the hotplate in N_2 filled glove box (isolating the effects of moisture, oxygen and light) at various temperatures (100 ^{o}C, 150 ^{o}C and 250 ^{o}C). After thermal stress, Calcium and aluminum contacts were formed by vacuum deposition at pressures below 3 x 10^{-6} Torr. All device fabrication procedures and measurements were carried out in air at room temperature.

Device fabrication for light and air stability: the inverted device structure is employed with indium tin oxide (ITO)/zinc oxide (ZnO)/polyethylenimine ethoxylated (PEIE)/photo-active layer (*d* = ~100 nm)/molybdenum oxide(MoO_3)/Ag for the light and air stability test. Glass

substrates were used with pre-patterned ITO. These were cleaned by sonication in detergent, deionized water, acetone and isopropanol in the sonication bath. ZnO (sol-gel or NPs) layers were deposited by spin coating of the respective solution followed by annealing at 150 ^{o}C for 10~15 min, giving layers of 30 nm thickness. The photo-active layers (d = ~100nm) were deposited from 15mg ml^{-1} solutions in chloroform (1mL) by spin coating at 2,000 r.p.m. Top electrode of the MoO_X (10 nm) and Ag (100 nm) layers were deposited by thermal evaporation at pressures below 3 x 10^{-6} Torr.

Photostability test: all devices with glass to glass encapsulation were stored in a humidity and temperature control chamber equipped with a sulfur plasma lamp and a computer-controlled voltage source measure unit for in situ current density–voltage (*J–V*) measurements. For the photodegradation test, the samples were exposed to light of intensity~ 100 mW cm^{-2} from the sulfur plasma lamp in air for 200 h. These conditions were applied for all photodegradation treatments used in this work. All samples were illuminated through the ITO. Devices were always stored at short-circuit except during periodic *J–V* scans. *J–V* scans at predetermined intervals were controlled by a computer program and resulting values for J_{SC}, V_{OC}, *FF* were automatically recorded. The light intensity of ~ 100 mW cm^{-2} was estimated by measuring the photocurrent from a silicon photodiode and assuming AM 1.5 spectral distribution. However, as the illumination spectrum is not the same as the AM 1.5 solar spectrum, we present the performance parameters during degradation after normalizing to their initial values.

Air stability: The air stability of BDT2TR:PC_{71}BM and BDT2TR:PNDI-2T devices was studied by keeping them out of the glove box without encapsulation. Devices were stored at room temperature, under the dark for 10 days.

SCLC devices fabrication and testing

Mobility measurements of oligomer/$PC_{71}BM$ (w/w, 1.0:1.0), and oligomer:PNDI-2T blends were done by a charge-only space-charge limited current (SCLC) method with the following diode structures: ITO/PEDOT:PSS/active layer/Au for hole-only devices and ITO/ZnO NPs/active layer/Ca/Al for electron-only devices by taking current-voltage measurements and fitting the results to a space-charge limited form. The charge carrier mobilities were calculated using the SCLC model, where the SCLC is described by: $9\varepsilon_0\varepsilon_r\mu V^2/8L^3$, where *J* is the current density, L is the film thickness of the active layer, μ_0 is the hole or electron mobility, ε_r is the relative dielectric constant of the transport medium, ε_0 is the permittivity of free space (8.85×10^{-12} F m^{-1}), V is the internal voltage in the device, and $V = V_{appl} - V_r - V_{bi}$, where V_{appl} is the applied voltage to the device, V_r is the voltage drop due to contact resistance and series resistance between the electrodes, and V_{bi} is the built-in voltage due to the relative work function difference of the two electrodes.

Synchroton X-ray Diffraction Analysis

Grazing-incidence XRD (GIXD) measurements were conducted at PLS-II 9A U-SAXS beamline of Pohang Acceleartor Laboratory (PAL) in Korea. The X-rays coming from the in-vacuum undulator (IVU) are monochromated using Si(111) double crystals and focused at the detector position using K-B type mirrors. GIXD patterns were recorded with a 2D CCD detector (Rayonix SX165) and X-ray irradiation time was 2 ~ 120 seconds dependent on the saturation level of detector. Diffraction angles were calibrated by a pre-calibrated sucrose (Monoclinic, P21, a = 10.8631 Å, b = 8.7044 Å, c = 7.7624 Å, b = 102.938o) and the sample-to-detector distance was about 223.2 mm.

Flexible device fabrication

PET/ITO substrates were used for flexible devices. After spin coating PEDOT:PSS on PET/ITO substrate at 4000 rpm for 60 s, the samples were dried on hotplate at 100 ^oC for 20 min. The

active area was fixed at 0.16 cm^2. All devices fabrication except Ca/Al (~100 nm) deposition and measurement was conducted at air condition under controlled relative humidity below 35 %.

Photoluminescence (PL) spectroscopy

Thin films were excited at 600 nm or 400nm with a solid state laser in continuous wave operation (MGL-III-532, Changchun New Industries) at an excitation power of 80 mW. The laser beam was expanded to a spot size of 6 mm in diameter in order to probe a rather large sample volume. Photoluminescence was fiber-coupled into a spectrograph (Acton Research SpectraPro 300i) and detected with an intensified CCD (Princeton Research, PiMax 512). The thickness of all films is identical for accuracy of the PL quenching efficiency.

1 S. Badgujar, G.-Y. Lee, T. Park, C. E. Song, S. Park, S. Oh, W. S. Shin, S.-J. Moon, J.-C. Lee, S. K. Lee, *Adv. Energy Mater*., 2016, **6**, 1600228.

2. S. A. Gevorgyan, M. Jørgensen and F. C. Krebs, *Sol. Energy Mater. Sol. Cells*, 2008, **92**, 736.

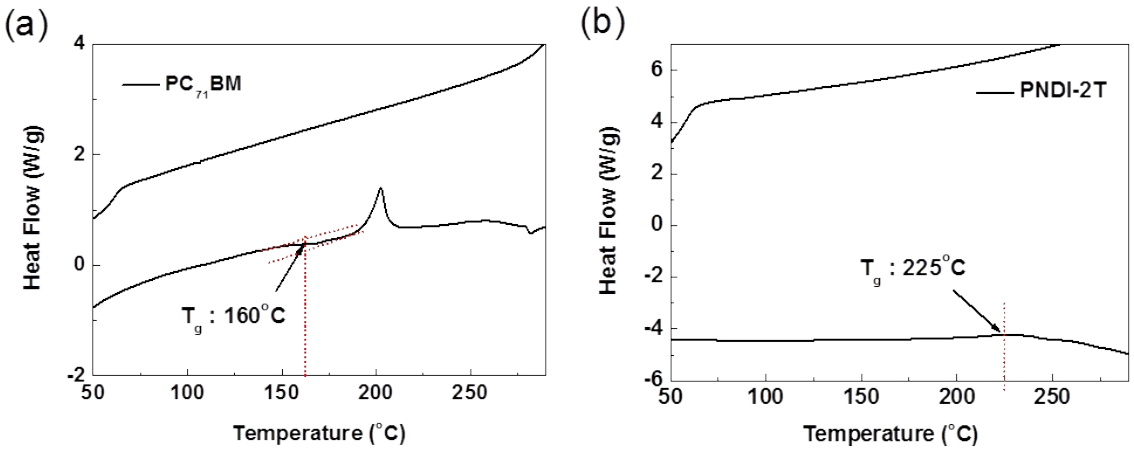

Fig. S1 DSC thermogram of (a) $PC_{71}BM$ and (b) PNDI-2T in a N_2 atmosphere at scan rate of 10 $^{o}C\ min^{-1}$.

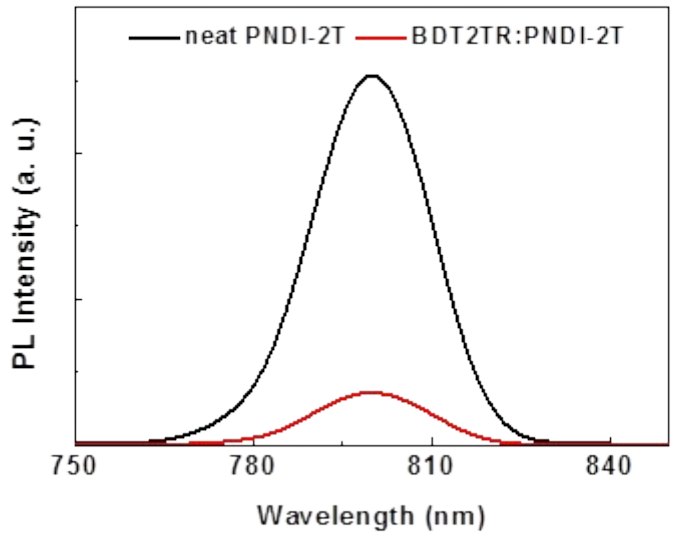

Fig. S2 PL spectra of neat PNDI-2T and blend in film state with excitation wavelength at 400 nm.

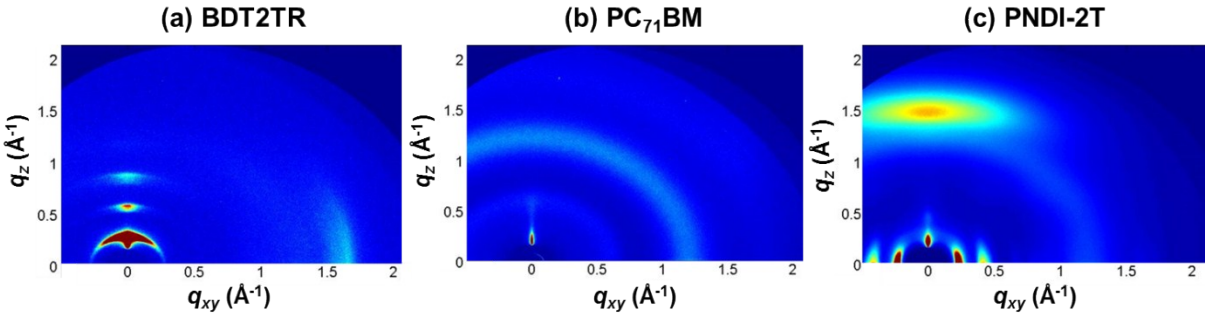

Fig. S3 2D GIWAXS image of pristine film of (a) BDT2TR, (b) $PC_{71}BM$, (c) PNDI-2T.

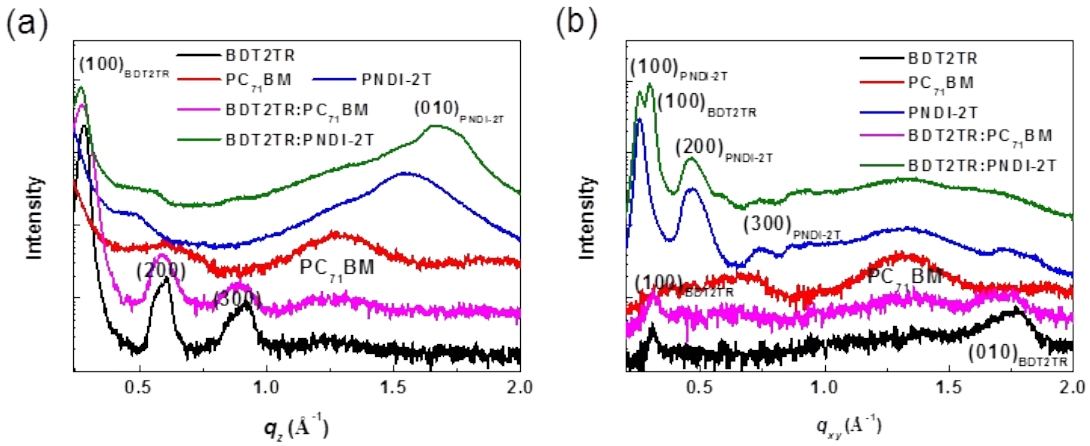

Fig. S4 Line-cuts profiles from neat of BDT2TR, $PC_{71}BM$, and PNDI-2T film, and blend of two film corresponding (a) out-of-plane, (b) in-plane.

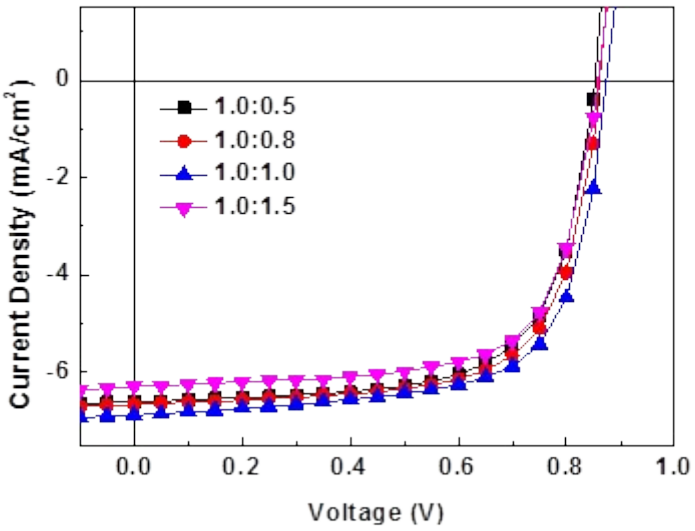

Fig. S5 The *J-V* curve of BDT2TR:PNDI-2T OSCs with different active layer blend ratios.

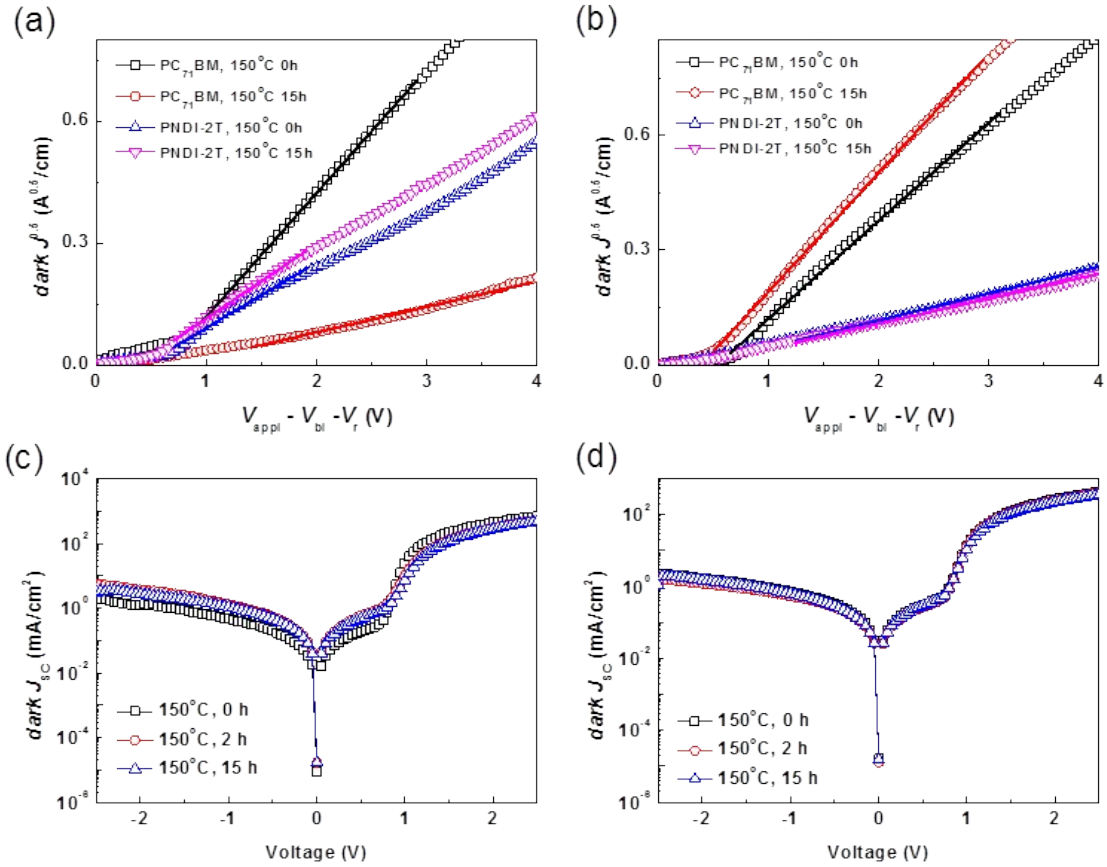

Fig. S6 The dark *J-V* curve of (a) hole-only and (b) electron-only device based on the BDT2TR:$PC_{71}BM$, BDT2TR:PNDI-2T blend film with annealing time, Dark *J-V* properties of (c) BDT2TR:$PC_{71}BM$ OSCs with different thermal stability processing of 0 h, 2 h, and 15 h, (d) BDT2TR:PNDI-2T OSCs with different thermal stability processing of 0 h, 2 h, and 15 h.

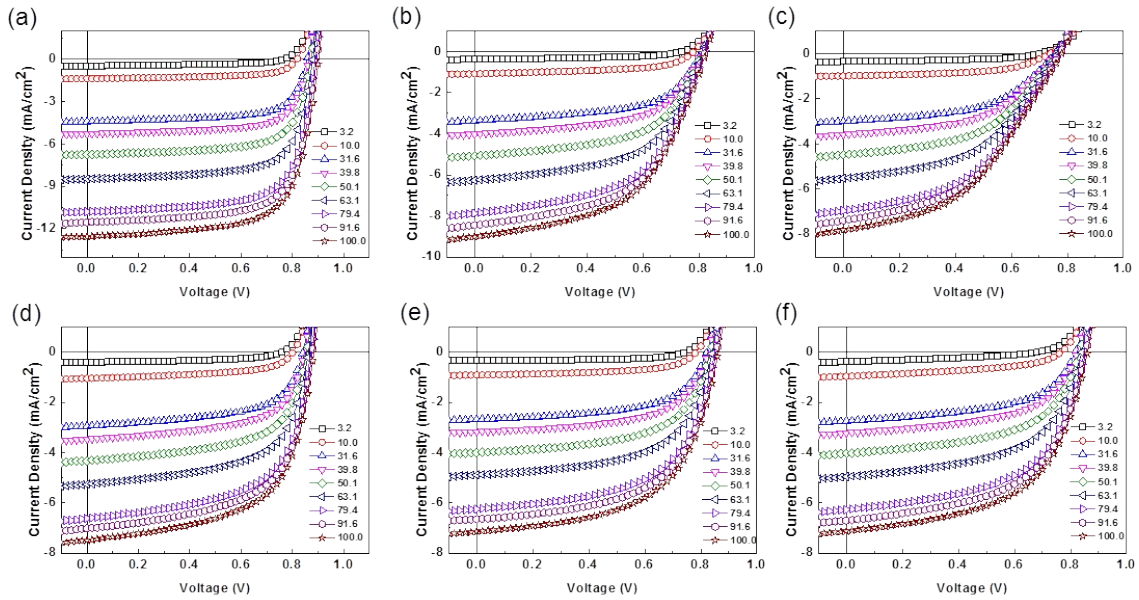

Fig. S7 *J–V* curves of OSCs based on (a) BDT2TR:$PC_{71}BM$ (b) BDT2TR:PNDI-2T processed with without thermal stress, (b), (e) with thermal processing at 150 °C for 2h, (c),(f) at 150 °C for 15 h under a light intensity of 3.2~100 mW cm^{-2}.

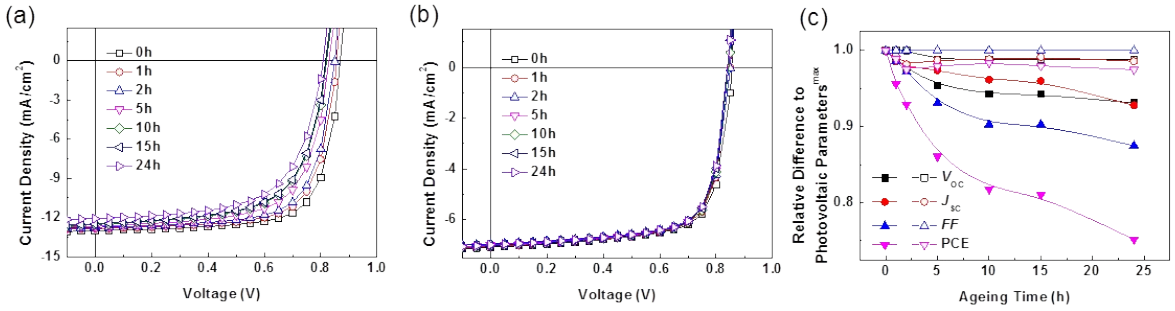

Fig. S8 *J–V* curves of OSCs based on (a) BDT2TR:$PC_{71}BM$ (b) BDT2TR:PNDI-2T processed with thermal stress at 100 °C (c) solar cell performance thermal stability at 100 °C based on the BDT2TR:$PC_{71}BM$ (filled) and BDT2TR:PNDI-2T device (unfilled).

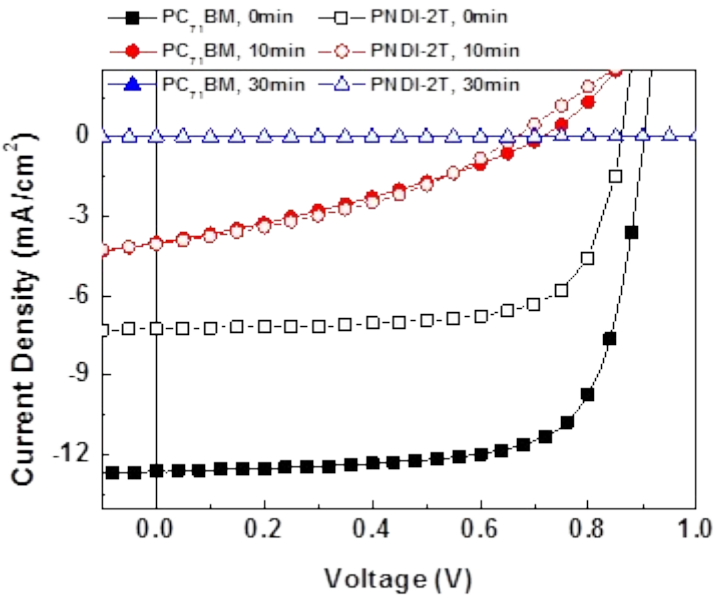

Fig. S9 *J–V* curves of OSCs based on a BDT2TR:$PC_{71}BM$ (filled) and BDT2TR:PNDI-2T (unfilled) processed with thermal stress at 250 °C.

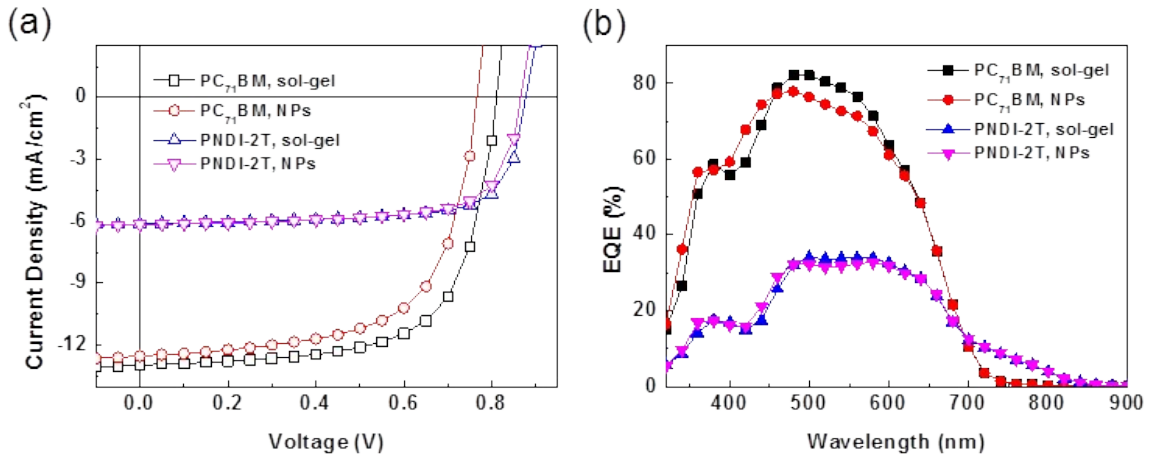

Fig. S10 (a) The *J–V* curves and (b) EQE spectra of inverted device of initial performance of BDT2TR:$PC_{71}BM$, and BDT2TR:PNDI-2T from different ZnO (sol-gel & NPs) for light stability test.

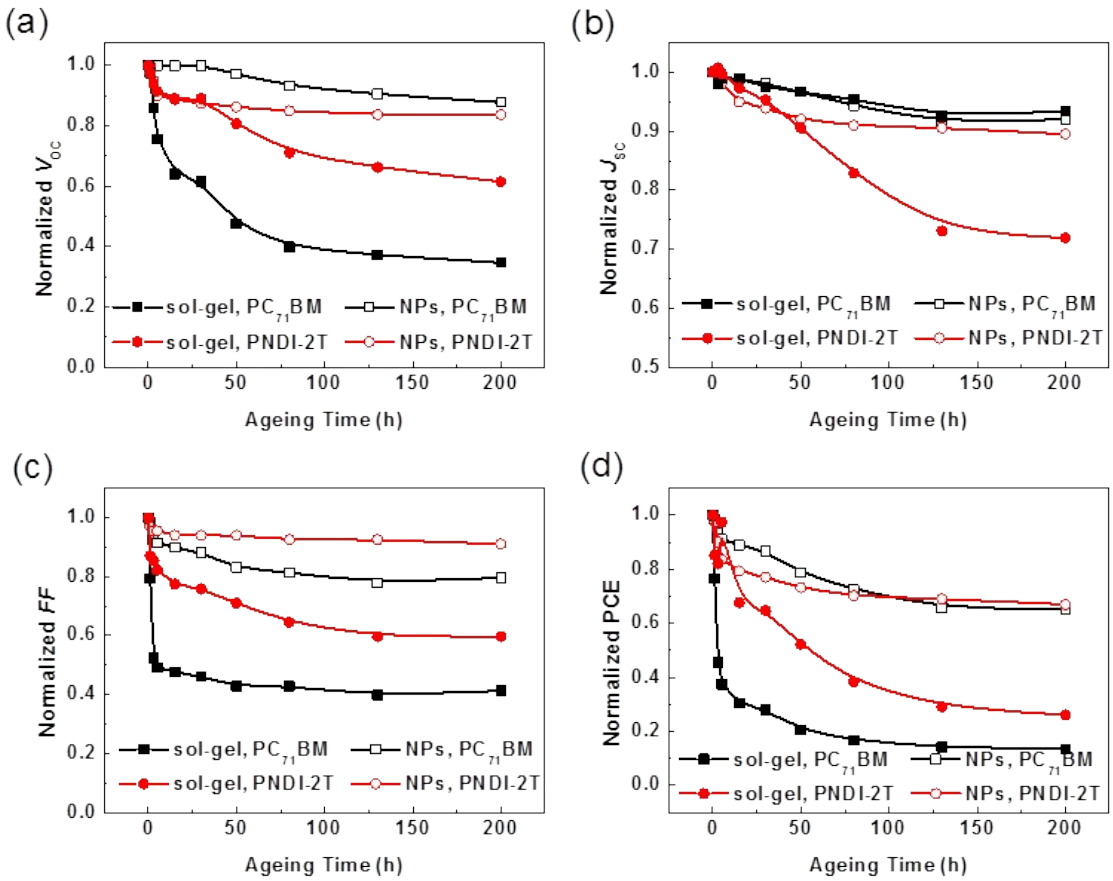

Fig. S11 Photovoltaic parameters of (a) V_{OC}, (b) J_{SC}, (c) *FF*, (d) PEC based on BDT2TR:$PC_{71}BM$ and BDT2TR:PNDI-2T films under continuous illumination (1.5 AM, 100 mW/cm^2) for 200 h.

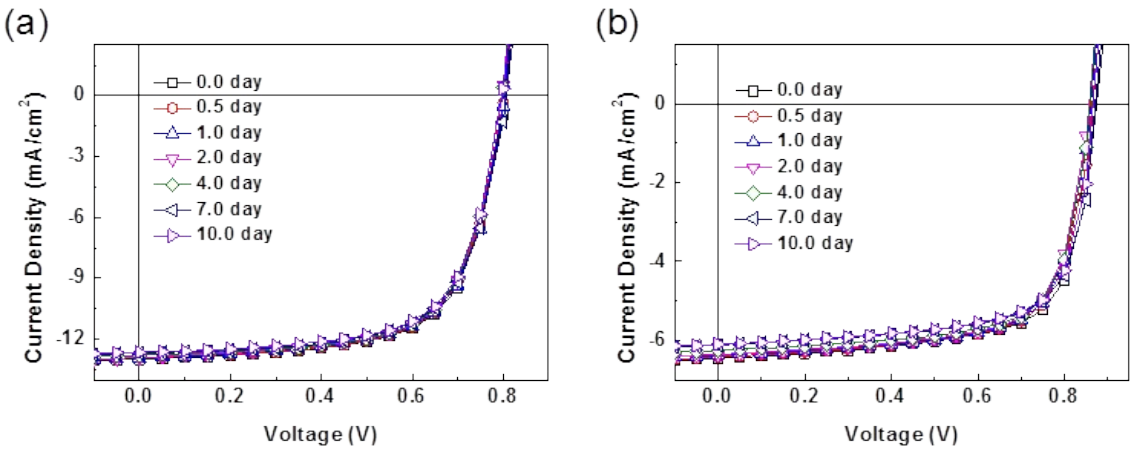

Fig. S12 The *J*–*V* curves of BDT2TR:Acceptor device from (a) $PC_{71}BM$, (b) PNDI-2T. Inverted devices are ITO/sol-gel ZnO/BDT2TR:Acceptor/MoO_x/Ag and stored in the dark under ambient conditions for 10 days.

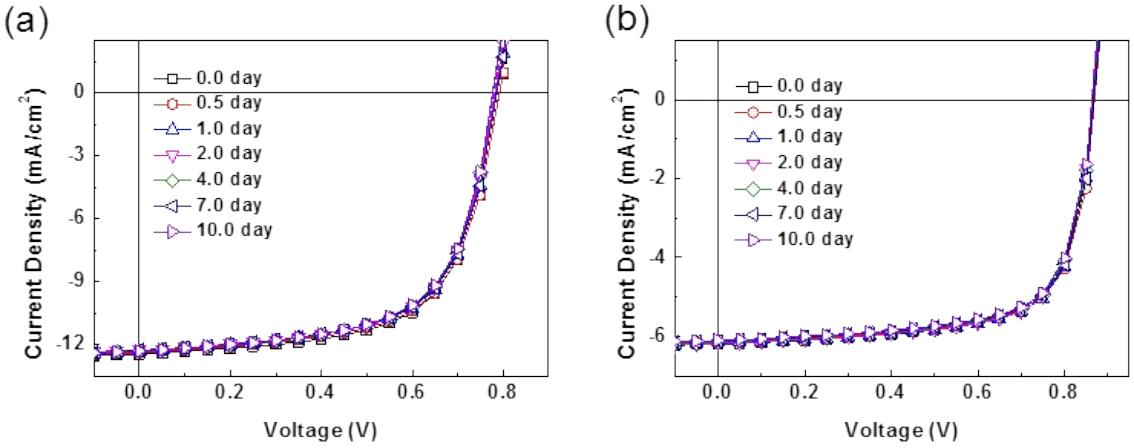

Fig. S13 The *J*–*V* curves of BDT2TR:$PC_{71}BM$ device from different ZnO (a) sol-gel, (b) NPs. Devices were stored in the dark under ambient conditions for 10 days.

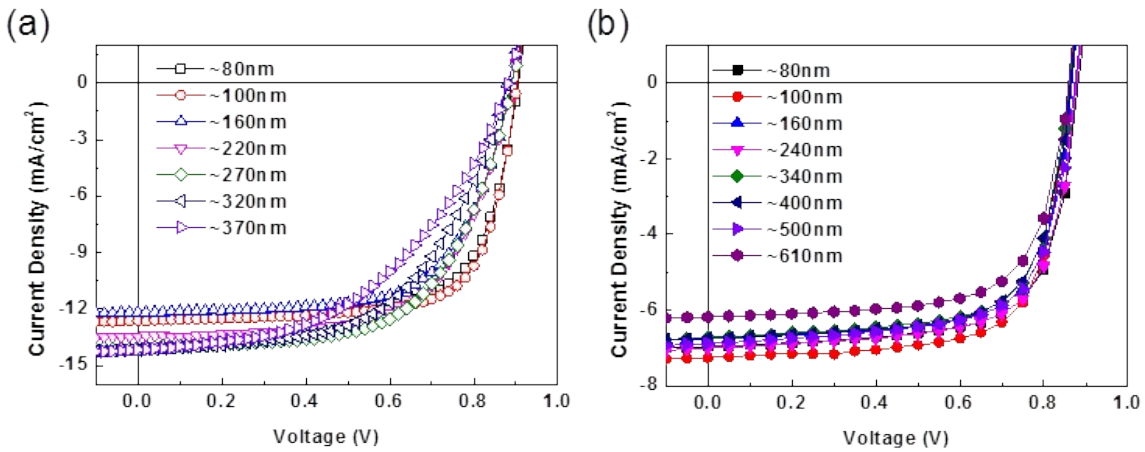

Fig. S14 The *J-V* curve of (a) BDT2TR:$PC_{71}BM$ (b) BDT2TR:PNDI-2T OSCs with different active layer thickness.

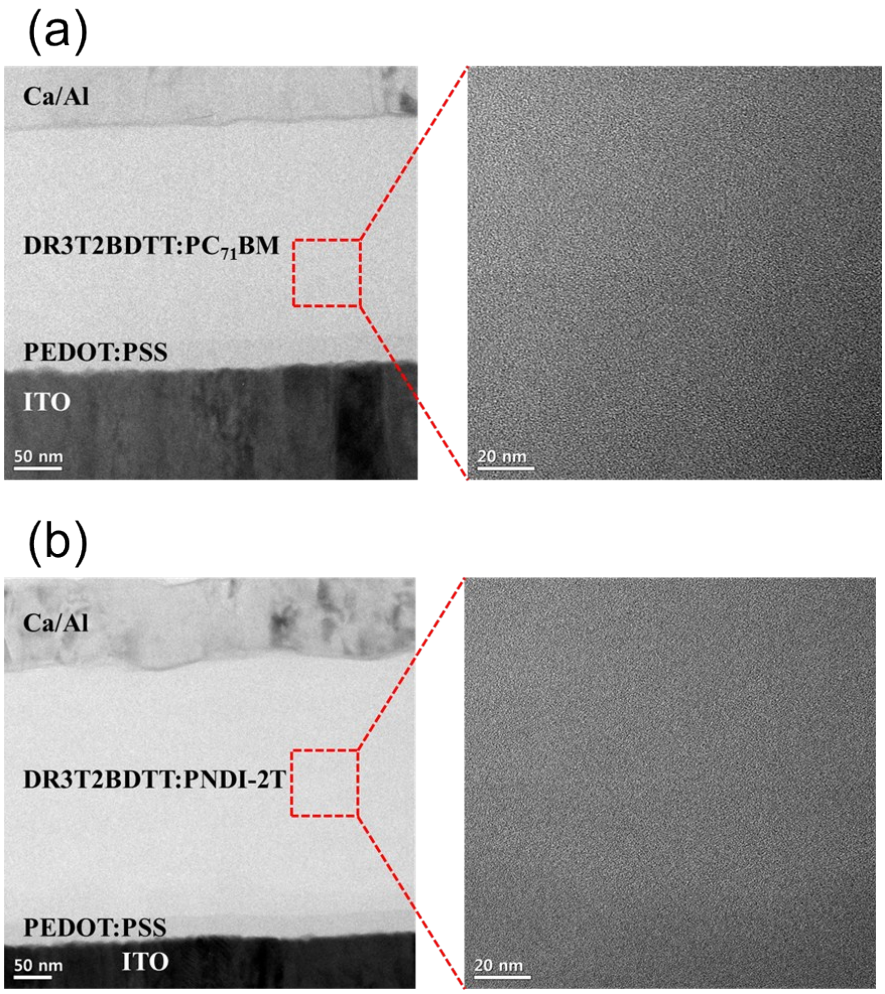

Fig. S15 The cross-section TEM imaged of (a) BDT2TR:$PC_{71}BM$ OSCs with 360nm active layer thickness (b) BD2TR:PNDI-2T OSCs with 610nm active layer thickness.

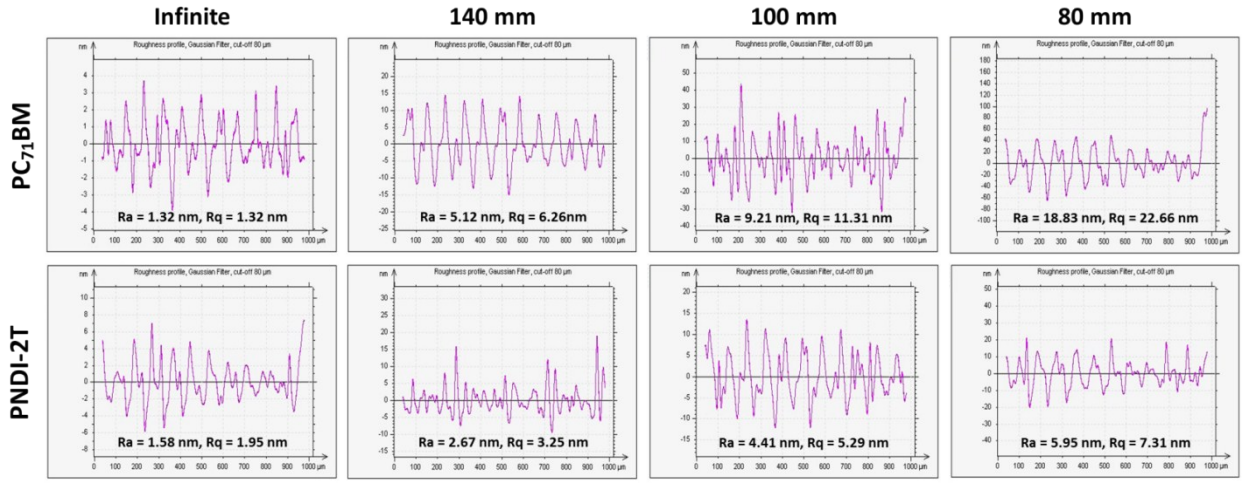

Fig. S16 The surface profile of the relevant bending test based on BDT2TR:$PC_{71}BM$ and BDT2TR:PNDI-2T OSCs with different bending radius per each 100 cycles.

Table S1. Packing parameters od pristin active materials and blen two OSCs derived from GIWXS measurements.

Active Layer	Component	(100) $d_{lamellar}$ [Å][a]	(010) $d_{\pi-\pi}$ [Å][a]	(100) $d_{lamellar}$ [Å][b]	(010) $d_{\pi-\pi}$ [Å][b]
BDT2TR	-	22.21	-	20.41	3.55
PNDI-2T	-	-	4.03	24.37	-
BDT2TR:$PC_{71}BM$	-	22.96	-	20.65	3.58
BDT2TR:PNDI-2T	BDT2TR	23.60	-	21.30	-
	PNDI-2T	-	3.77	24.73	-

[a]Calculation from *z*-axis.
[b]Calculation from *xy*-axis.

Table S2. Device characteristics BDT2TR:PNDI-2T OSCs with different D:A blend ratios under conventional device architecture ITO/PEDOT:PSS/Photo-active layer/Ca/Al.

Wight ratio [w/w]	V_{OC} [V]	J_{SC} [mA/cm^2]	*FF* [%]	PCE [%]
1.0:0.5	0.85	6.61	68	3.83
1.0:0.8	0.86	6.68	69	3.96
1.0:1.0	0.86	7.26	71	4.43
1.0:1.5	0.85	6.29	69	3.75

Table S3 Photovoltaic properties of the BDT2TR:$PC_{71}BM$ and BDT2TR:PNDI-2T device under thermal stress at 100 °C for 24 h in N_2 filled glove box.

Acceptor	Time [h]	V_{OC} [V]	J_{SC} [mA/cm^2]	*FF* [%]	PCE[a] [%]
$PC_{71}BM$	0	0.87	13.03	72	8.17 (8.03)[b]
	1	0.86	12.84	71	7.81 (7.70)[b]
	2	0.85	12.76	70	7.59 (7.42)[b]
	5	0.83	12.69	67	7.03 (6.89)[b]
	10	0.82	12.53	65	6.68 (6.40)[b]
	15	0.82	12.51	65	6.62 (6.34)[b]
	24	0.81	12.09	63	6.14 (5.95)[b]
PNDI-2T	0	0.85	7.10	72	4.35 (4.24)[b]
	1	0.85	7.05	72	4.30 (4.22)[b]
	2	0.85	6.97	72	4.24 (4.14)[b]
	5	0.84	7.01	72	4.26 (4.18)[b]
	10	0.84	7.02	72	4.28 (4.19)[b]
	15	0.84	7.04	72	4.26 (4.16)[b]
	24	0.84	7.00	72	4.24 (4.12)[b]

[a]The device architecture is ITO/PEDOT:PSS/BDT2TR:Acceptor(*d* = ~100nm)/Ca/Al.
[b]The average PCE in the brackets is obtained from over 5 independent devices.

Table S4 Photovoltaic properties of a BDT2TR:$PC_{71}BM$ and BDT2TR:PNDI-2T device under thermal stress at 250 °C.

Acceptor	Time [min]	V_{oc} [V]	J_{sc} [mA/cm^2]	*FF* [%]	PCE[a] [%]
$PC_{71}BM$	0	0.90	12.62	72	8.20 (8.11)[a]
	10	0.71	4.01	32	0.91 (0.82)[a]
	30	0.03	0.00	00	0.00 (0.00)[a]
PNDI-2T	0	0.86	7.26	71	4.43 (4.30)[a]
	10	0.67	4.04	37	0.99 (0.89)[a]
	30	0.01	0.00	00	0.00 (0.00)[a]

[a]The device architecture is ITO/PEDOT:PSS/BDT2TR:Acceptor(*d* = ~100nm)/Ca/Al.
[b]The average PCE in the brackets is obtained from over 5 independent devices.

Table S5 The initial photovoltaic properties of a BDT2TR:$PC_{71}BM$ and BDT2TR:PNDI-2T device with different ZnO conditions for light stability test.

Acceptor	ZnO	V_{oc} [V]	J_{sc} [mA/cm^2]	*FF* [%]	PCE[a] [%]
$PC_{71}BM$	sol-gel	0.81	12.96 (12.54)[b]	67	7.04 (6.58)[c]
	NPs	0.77	12.55 (12.23)[b]	64	6.13 (5.02)[c]
PNDI-2T	sol-gel	0.88	6.13 (6.08)[b]	73	3.93 (3.85)[c]
	NPs	0.87	6.16 (6.07)[b]	71	3.78 (3.49)[c]

[a]The device architecture is ITO/ETL/PEIE/BDT2TR:Acceptor(*d* = ~100nm)/MoO_X/Ag.
[b]The value is calculated from EQE data.
[c]The average PCE in the brackets is obtained from over 5 independent devices.

Table S6 The photovoltaic properties of a BDT2TR:$PC_{71}BM$ and BDT2TR:PNDI-2T device with sol-gel ZnO. Devices were stored in the dark under ambient conditions for 10 days.

Acceptor	Time [day]	V_{oc} [V]	J_{sc} [mA/cm^2]	*FF* [%]	PCE [%]
$PC_{71}BM$	0.0	0.80	13.00	67	7.02
	0.5	0.80	12.91	67	6.95
	1.0	0.80	12.92	67	6.92
	2.0	0.80	12.90	67	6.87
	4.0	0.80	12.79	67	6.85
	7.0	0.81	12.70	67	6.82
	10.0	0.80	12.65	67	6.76
PNDI-2T	0.0	0.87	6.46	70	3.92
	0.5	0.86	6.41	70	3.85
	1.0	0.86	6.37	70	3.83
	2.0	0.86	6.35	70	3.80
	4.0	0.86	6.26	70	3.77
	7.0	0.87	6.12	71	3.77
	10.0	0.87	6.09	71	3.73

[a]The device architecture is ITO/sol-gel ZnO/PEIE/BDT2TR:Acceptor(*d* = ~100nm)/MoO_X/Ag.

Table S7 The photovoltaic properties of a BDT2TR:$PC_{71}BM$ and BDT2TR:PNDI-2T device with ZnO NPs. Devices were stored in the dark under ambient conditions for 10 days.

Acceptor	Time [day]	V_{oc} [V]	J_{sc} [mA/cm^2]	*FF* [%]	PCE [%]
$PC_{71}BM$	0.0	0.79	12.47	64	6.29
	0.5	0.79	12.39	64	6.24
	1.0	0.78	12.34	63	6.15
	2.0	0.78	12.27	64	6.13
	4.0	0.78	12.28	64	6.11
	7.0	0.79	12.29	63	6.12
	10.0	0.78	12.32	63	6.08
PNDI-2T	0.0	0.87	6.20	70	3.77
	0.5	0.87	6.16	70	3.76
	1.0	0.86	6.16	71	3.78
	2.0	0.86	6.18	70	3.76
	4.0	0.87	6.14	70	3.72
	7.0	0.87	6.11	70	3.73
	10.0	0.86	6.10	70	3.68

[a]The device architecture is ITO/ZnO NPs/PEIE/BDT2TR:Acceptor(*d* = ~100nm)/MoO_X/Ag.

Table S8. Conventional OSCs results of BDT2TR:$PC_{71}BM$ and BDT2RT:PNDI-2T with variable film thickness.

Acceptor	*d* [nm]	V_{OC} [V]	J_{SC} [mA/cm^2]	*FF* [%]	PCE [%]
$PC_{71}BM$	~360	0.88	14.16	48	6.04 (5.83)[a]
	~320	0.88	14.16	56	6.99 (6.80)[a]
	~270	0.89	14.13	61	7.67 (7.47)[a]
	~220	0.89	13.46	63	7.59 (7.38)[a]
	~160	0.89	12.18	65	7.08 (6.81)[a]
	~100	0.90	12.62	72	8.20 (8.11)[a]
	~80	0.91	12.43	70	7.91 (7.77)[a]
PNDI-2T	~610	0.86	6.18	69	3.67 (3.60)[a]
	~500	0.87	6.89	69	4.12 (4.02)[a]
	~400	0.86	6.75	69	4.04 (3.90)[a]
	~340	0.86	6.72	70	4.05 (3.90)[a]
	~240	0.88	7.01	70	4.28 (4.14)[a]
	~160	0.87	6.76	70	4.12 (4.03)[a]
	~100	0.86	7.26	71	4.43 (4.30)[a]
	~80	0.88	6.96	70	4.29 (4.18)[a]

[a]The average PCE in the brackets is obtained from over 5 independent devices.

Table S9. Photovoltaic properties of of BDT2RT:$PC_{71}BM$ and BDT2RT:PNDI-2T OSCs with various bending radius.

Acceptor	Bending radius	V_{oc} [V]	J_{sc} [mA/cm^2]	*FF* [%]	PCE [%]
$PC_{71}BM$	Infinite	0.90	12.57	65	7.33 (6.98)[a]
	140 mm	0.89	10.64	58	5.52 (5.13)[a]
	100 mm	0.88	9.70	52	4.43 (3.78)[a]
	80 mm	0.43	9.67	38	1.59 (0.99)[a]
PNDI-2T	Infinite	0.87	7.26	63	3.99 (3.71)[a]
	140 mm	0.87	7.16	61	3.81 (3.30)[a]
	100 mm	0.86	7.06	60	3.65 (3.22)[a]
	80 mm	0.86	6.09	61	3.20 (3.04)[a]

[a]The average PCE in the brackets is obtained from over 5 independent devices.